

Optimal Control of Isometric Muscle Dynamics

Robert Rockenfeller & Thomas Götz

Mathematical Institute, University Koblenz-Landau, Campus Koblenz Universitätsstr. 1, 56070 Koblenz, Germany Email: rrockenfeller@uni-koblenz.de

Abstract. We use an indirect optimal control approach to calculate the optimal neural stimulation needed to obtain measured isometric muscle forces. The neural stimulation of the nerve system is hereby considered to be a control function (input) of the system 'muscle' that solely determines the muscle force (output). We use a well-established muscle model and experimental data of isometric contractions. The model consists of coupled activation and contraction dynamics described by ordinary differential equations. To validate our results, we perform a comparison with commercial optimal control software.

Keywords: biomechanics; inverse dynamics; muscle model; optimal control, stimulation.

1 Introduction

Mathematical models for everyday phenomena often ask for a control or input such that a system reacts in an optimal or at least in a desired way. Whether finding the optimal rotation of a stick for cooking potatoes on the open fire such that the potato has a desired temperature, see [1], or computing the optimal neural stimulation of a muscle such that the force output is as close as possible to experimentally measured data. Typical examples for biomechanical optimal control problems occur in the calculation of goal directed movements, see [2-4] and in robotics [5]. Concerning huge musculoskeletal systems, the load sharing problem of muscle force distribution has to be solved using optimal control [6, 7]. The most common application for solving the load sharing problem is the inverse dynamics of multi-body systems (MBS) as in [8,9]. The aim is to approximate observed multi-body trajectories by a forward simulation. The problem occurs to find a set of muscle activations such that the muscle forces resulting from the MBS simulation are similar to the measured ones.

Considering a general optimal control problem there is a process described by a vector of state variables \mathbf{x} which has to be influenced by control variable $\mathbf{u} \in \mathcal{U}$ within a time interval $[t_0, t_1]$ such that a given objective function $\mathfrak{I}(\mathbf{x}, \mathbf{u})$ is minimized subject to the model equations. These model equations can be either ordinary differential equations (ODE), partial differential equations (PDE) or differential algebraic equations (DAE). Additional constraints on the control

variable as well as the state variable itself can be imposed. The corresponding general optimal control problem reads as follows:

$$min_{u} \Im(\mathbf{x}, u) = \int_{t_{0}}^{t_{1}} j(\mathbf{x}(u, t), u(t), t) dt$$
subject to
$$\dot{x} = f(\mathbf{x}, u, t)$$

$$0 = g(\mathbf{x}, u, t)$$

$$\mathbf{x} \in [x_{min}, x_{max}], \qquad u \in \mathcal{U}, \mathbf{x}(t_{0}) = \mathbf{x}_{0}$$
(Constraints)

For solving this minimization problem we introduce an adjoint (or costate) variable λ which operates as a penalty function, if the ODE or DAE are not fulfilled. The optimized control variable u^* is found at the saddle point of the Lagrangian \mathcal{L} .

$$\mathcal{L}(\mathbf{x}, \mathbf{u}, \lambda) = \int_{t_0}^{t_1} \mathbf{j}(\mathbf{x}(\mathbf{u}, t), \mathbf{u}(t), t) + \lambda_1(t) \left[\dot{\mathbf{x}} - \mathbf{f}(\mathbf{x}, \mathbf{u}, t)\right] + \lambda_2(t) \mathbf{g}(\mathbf{x}, \mathbf{u}, t) dt$$
subject to
$$\mathbf{x} \in [\mathbf{x}_{\min}, \mathbf{x}_{\max}], \quad \mathbf{u} \in \mathcal{U}, \quad \mathbf{x}(t_0) = \mathbf{x}_0$$
 (2)

Almost exclusively in biomechanical literature, the problem in Eq. (1) is solved by the technique of *first discretize then optimize* also known as direct method. Therefore \Im as well as the ODE/DAE constraints are discretized on a given time grid resulting in a huge non-linear program (NLP), see [1, 10-12]. For solving such NLPs, several efficient solvers have been designed. In [9] the program DIRCOL (DIRect COLlocation) from [13] is used. But for state-of-the-art programming MATLAB based packages exist like: GPOPS2 (General Pseudospectral Optimal Software) [14] or TOMLAB's developments SNOPT (Sparse Linear OPTimizer) and PROPT (Per Rutquist OPTimizer) in [15]. Those solvers commonly use a (pseudo–)gradient based method like BFGS or other quasi–Newton methods for minimizing the objective function.

However, we want to apply the approach of *first optimize then discretize*. Therefore we derive the first order necessary conditions for problem in Eq. (2) explicitly. We obtain the optimal control u* by solving the upcoming coupled ODE/DAE system. A state-of-the-art solver for the so-called indirect method (BNDSCO) was developed by [16]. The name BNDSCO indicates the use on boundary value problems with switching conditions. This solver uses a multiple shooting method to solve the resulting boundary value problem. For an enhanced discussion on both *first discretize then optimize* and *first optimize then discretize* approaches, see [11,13,17].

Most of the available literature on optimal control of muscle dynamics does not involve more control than just the level of activation, see [9]. However, we

choose a control on a deeper physiological level, namely the neural stimulation, to find an optimal neural stimulation such that the observed muscle forces are recovered. Furthermore we want to think of the neural stimulation as a continuous function rather than a bang–bang impulse as in [18].

The biomechanical applications of our method are multifaceted. At first it is an additional validation for the used muscle model because a qualitative error (objective function value) can be given. Moreover, the method's findings allow an investigation of specific parts of the model, for example the passive and active force—length curves as well as the activation dynamics. Regaining the optimal stimulation of an isometric contraction additionally reveals information about internal concentric and eccentric contraction processes where the latter is normally hard to investigate solely, see [19]. Furthermore we obtain indications for model improvements such as the need to include the concept of fatigue as suggested in [20].

In Section 2 we recapitulate the muscle model given in [21] using contraction modes from [22]. For simplicity, we just consider the situation for a single muscle. In Section 3 we formally derive the first order optimality conditions and present an iterative solution algorithm for the upcoming coupled state—costate—system. Our results are presented in Section 4. In Section 5 we compare our finding with the output of the above mentioned commercial software PROPT. The paper closes with an outlook on possible future work.

2 Model Description and Problem Formulation

In this paper we use a modified *Hill-model* [21,22] to describe the contraction motion of muscles. This model is based on a mechanical analogy of the muscle tendon complex (MTC) and is constituted by four basic compartments. The contractile element (CE) produces the force by contracting, or more precisely by actin-myosin cross-bridges at the sarcomere level. The parallel elastic element (PEE) represents the connective tissues and is responsible for the muscle passive behavior. The serial elastic element (SEE) represents the elastic behavior of the tendon connecting the muscle to the skeleton. The serial damping element (SDE) describes the viscous damping of the tendon.

2.1 Model Description

Let ℓ_{MTC} , ℓ_{PEE} , ℓ_{CE} , ℓ_{SEE} and ℓ_{SDE} denote the length of the constituting elements. Due to the setup of the model the following restrictions hold:

$$\ell_{\rm CE} = \ell_{\rm PEE}$$
, $\ell_{\rm SEE} = \ell_{\rm SDE}$ and $\ell_{\rm MTC} = \ell_{\rm CE} + \ell_{\rm SEE}$.

Using the notation F_i for the force acting on the i–th component, at equilibrium it holds that

$$F_{MTC} = F_{CE} + F_{PEE} = F_{SEE} + F_{SDE} . (3)$$

In the sequel we shortly outline the individual force equations, details can be found in [22]. For the reader not familiar with the biomechanical terminology, we recall that *isometric contraction* refers to the situation, where the muscle exerts some force without a change of length. In contrast to that, we speak of a *concentric* or *eccentric* contraction if the CE exerts force and shortens or elongates.

Following [22], we define the relation between the isometric force F_{isom} and the length ℓ_{CE} of the muscle

$$F_{isom}(\ell_{CE}) = \begin{cases} \exp\left(-\left|\frac{\ell_{CE} - \ell_{CEopt}}{\ell_{CEopt} \Delta W_{asc}}\right|^{\nu_{asc}}\right), & \text{if } \ell_{CE} < \ell_{CEopt}, \\ \exp\left(-\left|\frac{\ell_{CE} - \ell_{CEopt}}{\ell_{CEopt} \Delta W_{des}}\right|^{\nu_{des}}\right), & \text{if } \ell_{CE} \ge \ell_{CEopt}. \end{cases}$$
(4)

The parameters ΔW_{asc} , ν_{asc} and ΔW_{des} , ν_{des} determine the width and slope of the two branches of the bell–shaped F_{isom} -curve. Note the normalization $F_{isom}(\ell_{CEopt}) = 1$ at the optimal length $\ell_{CE} = \ell_{CEopt}$, where the muscle is able to produce its maximum isometric force F_{max} . Other functional dependencies appear in literature, compare [23,24].

Subsequently we introduce the force-velocity relation of the contractile element

$$\begin{split} F_{\text{CE}} \left(\ell_{\text{CE}}, \dot{\ell}_{\text{CE}}, q \right) &= \\ & \left\{ \begin{array}{ll} F_{\text{max}} \left(\frac{q F_{\text{isom}} + a_{\text{rel}}}{1 - \dot{\ell}_{\text{CE}} / (b_{\text{rel}} \ell_{\text{CEopt}})} - a_{\text{rel}} \right), & \text{if } \dot{\ell}_{\text{CE}} < 0 & \text{(concentric),} \\ F_{\text{max}} \left(\frac{q F_{\text{isom}} + a_{\text{rel},e}}{1 - \dot{\ell}_{\text{CE}} / (b_{\text{rel},e} \ell_{\text{CEopt}})} - a_{\text{rel},e} \right), & \text{if } \dot{\ell}_{\text{CE}} \ge 0 & \text{(eccentric).} \\ \end{array} \end{split}$$

Note, that F_{CE} is non–differentiable at $\dot{\ell}_{CE}=0$. The variable q denotes the muscle activity. According to Zajac [25] the activity and the external neural stimulation σ are related via the ODE

$$\dot{\mathbf{q}} = \frac{1}{\tau} (\sigma - \sigma \cdot (1 - \beta) \cdot (\mathbf{q} - \mathbf{q}_0) - \beta \cdot (\mathbf{q} - \mathbf{q}_0)) . \tag{6}$$

The time constant τ and the activation–deactivation ratio β determine the velocity of activation growth or decay after a neural impulse. For a particular description of the physiological meaning of the occurring parameters see Appendix A or [22].

Another activation dynamics was given as a differential-algebraic system by Hatze [26]. A compact form of this system as a first order non-linear ODE was derived in [21,22]:

$$\dot{q}_{H} = \frac{v \cdot m}{1 - q_{0}} \cdot \left[\sigma \cdot \rho(\ell_{CErel}) \cdot \frac{(1 - q_{H})^{1 + 1/\nu}}{(q_{H} - q_{0})^{\frac{1}{\nu} - 1}} \cdot - (1 - q_{H}) \cdot (q_{H} - q_{0}) \right]. \quad (7)$$

The frequency m and the parameter ν were set by Hatze and depend on the particular muscle. The function $\rho(\ell_{CErel})$ is monotonically increasing and introduces a length-dependency of the activation. In [22] Hatze's activation dynamics is not used. However, [27] stated that Hatze's formulation might be physiologically more relevant than Zajac's. Hence, we want to include its impact in the discussion. For a detailed discussion of the above activation dynamics see [26].

Following [21,22] the parameters a_{rel} , $a_{rel,e}$, b_{rel} and $b_{rel,e}$ in Eq. (5) depend themselves on ℓ_{CE} and q via

$$a_{\text{rel}} = \begin{cases} \frac{a_{\text{rel},0}}{4}(1+3q), & \text{if } \ell_{\text{CE}} < \ell_{\text{CEopt}} \\ \frac{a_{\text{rel},0}}{4}(1+3q)F_{\text{isom}}, & \text{if } \ell_{\text{CE}} \ge \ell_{\text{CEopt}} \end{cases} \quad a_{\text{rel},e} = -F_e \, q \, F_{\text{isom}} \quad (8)$$

$$b_{rel} = \frac{b_{rel,0}}{7} (3 + 4q),$$
 $b_{rel,e} = \frac{b_{rel} (1 - F_e)}{S_e \left(1 + \frac{a_{rel}}{q \, F_{isom}}\right)}$ (9)

The parameter S_e is related to the ratio of the slopes at $\ell_{CE} = \ell_{CEopt}$ of the concentric and eccentric branch, see Eq. (5). The parameter $F_e = \lim_{\dot{\ell}_{CE} \to \infty} F_{CE} / (F_{max} \, q \, F_{isom})$ is related to the asymptotic behavior of the eccentric force. The parameters $a_{rel,0}$ and $b_{rel,0}$ refer to the Hill parameters, see [28].

For the two elastic elements we generally assume a non–linear behavior above a certain slack length $\ell_{\text{PEE},0}$ and $\ell_{\text{SEE},0}$

$$F_{\text{PEE}}(\ell_{\text{CE}}) = \begin{cases} 0, & \text{if } \ell_{\text{CE}} < \ell_{\text{PEE,0}}, \\ F_{\text{max}} \mathcal{F}_{\text{PEE}} \left(\frac{\ell_{\text{CE}} - \ell_{\text{PEE,0}}}{\ell_{\text{CEopt}} (1 + \Delta W_{\text{des}}) - \ell_{\text{PEE,0}}} \right)^{\nu_{\text{PEE}}}, & \text{if } \ell_{\text{CE}} \ge \ell_{\text{PEE,0}}. \end{cases}$$
(10)

The constant \mathcal{F}_{PEE} is related to the force F_{PEE} of the parallel elastic element at the length $\ell = \ell_{CEopt}(1 + \Delta W_{des})$ via $F_{PEE}(\ell) = F_{max}\mathcal{F}_{PEE}$.

Following [22], the serial elastic element is assumed to behave linearly, if its length exceeds a threshold $\ell_{\text{SEE,nll}}$:= $(1 + \Delta U_{\text{SEE,nll}})\ell_{\text{SEE,0}}$.

$$F_{SEE}(\ell_{SEE}) = \begin{cases} 0, & \text{if } \ell_{SEE} < \ell_{SEE,0} ,\\ \Delta F_{SEE,0} \left(\frac{\ell_{SEE} - \ell_{SEE,0}}{\Delta U_{SEE,nll} \ell_{SEE,0}} \right)^{\nu_{SEE}}, & \text{if } \ell_{SEE,0} \le \ell_{SEE} < \ell_{SEE,nll} ,\\ \Delta F_{SEE,0} \left(1 + \frac{\ell_{SEE} - \ell_{SEE,nll}}{\Delta U_{SEE,l} \ell_{SEE,0}} \right), & \text{if } \ell_{SEE} \ge \ell_{SEE,nll} . \end{cases}$$

$$(11)$$

The parameter $\Delta F_{SEE,0}$ refers to the force of the serial elastic element at length $\ell_{SEE,nll}$. The linear elastic regime for large length $\ell_{SEE} \geq \ell_{SEE,nll}$ is governed by the parameter $\Delta U_{SEE,l}$. The exponent of non-linearity for the serial elastic element is fixed by $\nu_{SEE} = \frac{\Delta U_{SEE,nll}}{\Delta U_{SEE,l}}$, whereas the exponent for the parallel elastic element is an adjustable model parameter, in this work we choose $\nu_{PEE} = \nu_{SEE}$, compare [22].

For the damping element SDE we assume a linearly increasing damping force

$$F_{SDE}(\dot{\ell}_{MTC}, \ell_{CE}, \dot{\ell}_{CE}, q) = D_{SDE}\left((1 - R_{SDE})\frac{F_{CE} + F_{PEE}}{F_{max}} + R_{SDE}\right)(\dot{\ell}_{MTC} - \dot{\ell}_{CE})$$
(12)

with damping parameters D_{SDE} at $F_{MTC} = F_{CE} + F_{PEE} = F_{max}$ and R_{SDE} at $F_{MTC} = 0$.

Solving the equilibrium Eq. (3) for the contraction velocity $\dot{\ell}_{CE}$ we obtain the following differential equation

$$\dot{\ell}_{CE} = \begin{cases} \frac{-C_1 - \sqrt{C_1^2 - 4C_2C_0}}{2C_2}, & \text{if } \dot{\ell}_{CE} < 0, \\ \frac{-C_{1,e} + \sqrt{C_{1,e}^2 - 4C_{2,e}C_{0,e}}}{2C_{2,e}}, & \text{if } \dot{\ell}_{CE} \ge 0. \end{cases}$$
(13)

The coefficients C_0 , C_1 and C_2 are given by

$$C_{0} = D_{0}\dot{l}_{MTC} + l_{CEopt}b_{rel}(F_{SEE} - F_{PEE} - F_{max}qF_{isom}),$$

$$C_{1} = -(C_{2}\dot{l}_{MTC} + D_{0} + F_{SEE} - F_{PEE} + F_{max}a_{rel}),$$

$$C_{2} = d_{SE,max}\left(R_{SDE} - \left[a_{rel} - \frac{F_{PEE}}{F_{max}}\right](1 - R_{SDE})\right).$$
(14)

The coefficients $C_{0,e}$, $C_{1,e}$, and $C_{2,e}$ in the eccentric case $\dot{l}_{CE} \geq 0$ are obtained when replacing a_{rel} , b_{rel} with $a_{rel,e}$, $b_{rel,e}$. The auxiliary coefficients $d_{SE,max}$ and D_0 are given by

$$d_{SE,max} = D_{SDE} \frac{F_{max} a_{rel,0}}{l_{CEopt} b_{rel,0}},\tag{15}$$

$$D_0 = l_{CEopt} b_{rel} d_{SE,max} \left(R_{SDE} + (1 - R_{SDE}) \left(q F_{isom} + \frac{F_{PEE}}{F_{max}} \right) \right). \tag{16}$$

Summarizing, Eqs. (3)-(13), we obtain a coupled system of equations allowing us to write the muscle force F_{MTC} as a function of the neural stimulation σ , i.e. $F_{MTC} = F_{MTC}(\sigma)$.

2.2 Problem Formulation

In [22] all model parameters stated above were estimated on the basis of experiments by [29] namely isometric contractions. In the experimental setup, conducted on piglet muscle, all conditions were controlled. The neural stimulation σ was imposed by an external electrical 0/1-impulse

$$\overline{\sigma}(t) = \begin{cases} 1, & \text{if } t \in [t_{\text{start}}, t_{\text{end}}] = [0.1 \text{ s}, 1.1 \text{ s}], \\ 0, & \text{else}. \end{cases}$$

$$(17)$$

As output information the resulting isometric force was measured at different fixed lengths ℓ_{MTC} of the muscle, see [22, Figure 7].

We address the following scenario: Assume we are not able to apply or measure the stimulation σ directly, but only measure the force resulting from isometric contraction. Are we able to reconstruct the stimulation $\sigma(t)$? In other words: We wish to find a stimulation $\sigma^*(t)$ such that the resulting force $F_{MTC}^* = F_{MTC}(\sigma^*)$ is as close as possible to the experimentally measured force denoted by \overline{F}_{MTC} .

Based on the previous muscle model we may notate this problem as a constrained minimization problem. Let $\mathcal{U} = C([0,T],[0,1])$ denote the continuous functions from time interval [0,T] which are bounded by [0,1]

$$\min_{\sigma \in \mathcal{I}} \Im(F_{MTC}, \sigma) = \frac{1}{2} \|F_{MTC} - \bar{F}_{MTC}\|_{L^2} + \frac{\alpha}{2} \|\sigma\|_{L^2}$$
 (18)

subject to the constraints

$$\dot{\mathbf{q}} = \mathbf{f}_1(\mathbf{q}, \mathbf{\sigma}), \qquad \qquad \mathbf{q}(0) = \mathbf{q}_0, \tag{19a}$$

$$\dot{\ell}_{CE} = f_2(\ell_{MTC}, \dot{\ell}_{MTC}, \ell_{CE}, q), \quad \ell_{CE}(0) = \ell_{CE,0},$$
 (19b)

$$\dot{\ell}_{\text{MTC}} = 0, \qquad \qquad \ell_{\text{MTC}}(0) = \ell_{\text{MTC},0} \,, \tag{19c}$$

$$F_{MTC} = f_3(\ell_{MTC}, \dot{\ell}_{MTC}, \ell_{CE}, q)$$
 (19d)

The constraint $\dot{\ell}_{\rm MTC} = 0$ in Eq. (19c) arises from the isometric contraction scenario. If other contraction types, e.g. quick release, are considered, this condition has to be replaced by the respective equations.

3 Solution and Results

Minimizing a cost functional \Im with respect to a control σ and subject to constraints given by a set of differential or algebraic conditions is a well-known and well-investigated problem. In this paper we will not go into details of proving the existence or uniqueness of minimizers, but rather formally derive the first order necessary conditions for the optimum.

In the isometric case $\ell_{MTC} = \ell_{MTC,0}$ is constant, therefore we skip this variable henceforth. Using this simplification, let us denote the state variable by $x = (F_{MTC}, q, \ell_{CE})$. Introducing the adjoint variable $\lambda = (\lambda_{F_{MTC}}, \lambda_q, \lambda_{\ell_{CE}})$, we formally define the Lagrangian

$$\mathcal{L}(x, \lambda, \sigma) :=$$

$$\mathfrak{J}(x,\sigma) + \langle \lambda_{F_{MTC}}, F_{MTC} - f_3 \rangle_{L^2} + \langle \lambda_q, \dot{q} - f_1 \rangle_{L^2} + \langle \lambda_{\ell_{CE}}, \dot{\ell}_{CE} - f_2 \rangle_{L^2} \ . \tag{20}$$

By $\langle u, v \rangle_{L^2} := \int_0^T u(t) \, v(t) \, dt$ we denote the usual L^2 -inner product. We use $D_{\widetilde{u}}u$ for the (Gâteaux) derivative of u in the direction of \widetilde{u} and use $\partial_t u$ for the partial derivative of u with respect to t.

The necessary first order optimality conditions imply that at a local optimum all (Gâteaux) derivatives of \mathcal{L} vanish. Computing formally the derivatives with respect to the adjoint variables $\lambda_{F_{MTC}}$, λ_{q} , $\lambda_{\ell_{CE}}$ we recover the state system

$$D_{\lambda_0} \mathcal{L} = 0 \Rightarrow \dot{q} = f_1(q, \sigma), \quad q(0) = q_0, \tag{21a}$$

$$D_{\lambda_{\ell_{\text{CE}}}}\mathcal{L} = 0 \ \Rightarrow \quad \dot{\ell}_{\text{CE}} = f_2(\ell_{\text{MTC}}, \ell_{\text{CE}}, q), \quad \ \ell_{\text{CE}}(0) = \ell_{\text{CE}, 0}, \quad \ (21b)$$

$$D_{\lambda_{F_{MTC}}} \mathcal{L} = 0 \implies F_{MTC} = f_3(\ell_{MTC}, \ell_{CE}, q). \tag{21c}$$

Taking derivatives with respect to the state variables F_{MTC} , q, ℓ_{CE} leads to a system of equations for the adjoint or costate:

$$D_{q}\mathcal{L} = 0 \Rightarrow \dot{\lambda}_{q} = -\lambda_{F_{MTC}} \partial_{q} f_{3} - \lambda_{\ell_{CF}} \partial_{q} f_{2} - \lambda_{q} \partial_{q} f_{1}, \ \lambda_{q}(T) = 0$$
 (22a)

$$D_{\ell_{CE}}\mathcal{L} = 0 \ \Rightarrow \ \dot{\lambda}_{\ell_{CE}} = -\lambda_{F_{MTC}} \, \partial_{\ell_{CE}} f_3 - \lambda_{\ell_{CE}} \, \partial_{\ell_{CE}} f_2, \ \lambda_{\ell_{CE}}(T) = 0 \eqno(22b)$$

$$D_{F_{MTC}} \mathcal{L} = 0 \Rightarrow \lambda_{F_{MTC}} = F_{MTC} - \overline{F}_{MTC}. \tag{22c}$$

The derivative with respect to the control σ gives rise to the gradient condition

$$D_{\sigma}\mathcal{L} = 0 \Rightarrow \qquad \alpha \, \sigma = \lambda_{q} \, \partial_{\sigma} f_{1} \,, \qquad 0 \le \sigma \le 1 \,.$$
 (23)

Note that the differential equations for the adjoint variables λ_q and $\lambda_{\ell_{CE}}$ have to be solved backwards in time, starting with the terminal conditions $\lambda_q(T)=0$ and $\lambda_{\ell_{CE}}(T)=0$. The functional expressions for the partial derivatives $\partial_q f_3$, etc. appearing in Eqs. (22a)-(23) can be derived explicitly, or at least symbolically in MATLAB. Using the Heaviside step function for expressing piecewise functions, these derivatives can be calculated in a closed form.

To solve the non-linear system of Eqs. (21)-(23), we use the iterative Algorithm 1. For the simulation results discussed in the next section, we implemented this algorithm using MATLAB (Version R2013b) including the symbolic toolbox for automatic computation of the partial derivatives and the pre–implemented ODE–solver ode45 for the numerical solution of the differential equations.

Figure 1 shows the results of the optimal control approach. Regarding Figure 1 (left) we compare the experimentally measured isometric forces \overline{F}_{MTC} (thin line, see [29]) with the force $F_{MTC}^*=F_{MTC}(\sigma^*)$ computed in the optimal control approach (bold line). Additionally, we have plotted the direct model output $F_{MTC}(\overline{\sigma})$ of the model Eq. (14) (dashed line) using the experimentally applied 0/1–stimulation $\overline{\sigma}$, see Eq. (17) . In Figure 1 (right) we show the reconstructed stimulation σ^* obtained by the optimal control approach versus time. The dashed line refers to the experimental input, i.e. the 0/1–impulse $\overline{\sigma}$. The results are plotted versus time for a muscle of given length $\ell_{MTC}=\ell_{MTC,ref}=6.15$ cm. In the subsequent Figure 2 this length serves as reference length.

```
Algorithm 1 Discretization after Optimization
```

```
Require: f_1, f_2, f_3, \overline{F}_{MTC}, \alpha, \ell_{MTC}, error tolerance Tol, initial guess \sigma_0 for the stimulation Calculate l_{CE,0} using Eq. (3)
```

Calculate F_{MTC} using $\sigma = \sigma_0$

while $\Im(F_{MTC}, \sigma) > Tol \ do$

Calculate $\lambda_{F_{MTC}} = F_{MTC} - \overline{F}_{MTC}$

Solve $\dot{\lambda}_{\ell_{CE}} = -\lambda_{F_{MTC}}\,\partial_{\,\ell_{CE}}f_3 - \lambda_{\ell_{CE}}\,\partial_{\,\ell_{CE}}f_2$ with $\lambda_{\ell_{CE}}(T) = 0$

Solve
$$\dot{\lambda}_q = -\lambda_{F_{MTC}}\,\partial_q f_3 - \lambda_{\ell_{CE}}\,\partial_q f_2 - \lambda_q\,\partial_q f_1$$
 with $\lambda_q(T) = 0$

Update σ via $\sigma=(1-\epsilon)\cdot\sigma+\frac{\epsilon}{\alpha}\cdot\lambda_q~\partial_\sigma f_1$ with convex combination factor ϵ

Solve $\dot{q} = f_1(q, \sigma_0)$ with $q(0) = q_0$

Solve $\dot{\ell}_{CE} = f_2(\ell_{MTC}, \dot{\ell}_{MTC}, \ell_{CE}, q)$ with $\ell_{CE}(0) = \ell_{CE,0}$

Calculate $F_{MTC} = f_3(\ell_{MTC}, \dot{\ell}_{MTC}, \dot{\ell}_{CE}, q)$

end while

Output F_{MTC} , ℓ_{CE} , $\dot{\ell}_{\text{CE}}$, q, $\sigma^* = \sigma$.

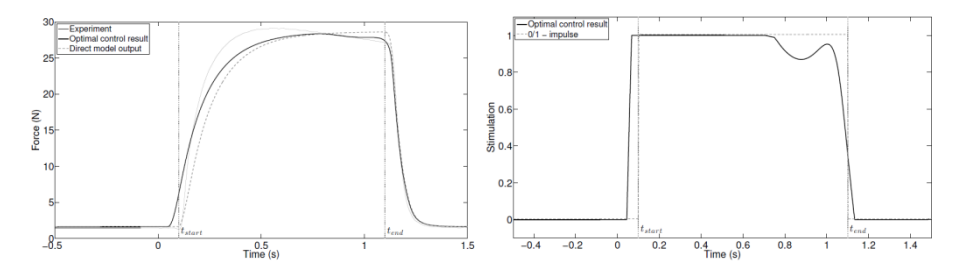


Figure 1 (Left) Isometric contraction forces vs. time: Experimental data [29] (thin), optimal control results F_{MTC}^* from Algorithm 1 (bold) and direct model output $F_{MTC}(\overline{\sigma})$ using (14) (dashed). The relative muscle length $l_{MTC}/l_{MTC,ref}=1$. In addition we have marked the starting time $t_{start}=0.1s$ and ending time $t_{end}=1.1s$ of the experimental reference stimulation $\overline{\sigma}$. (Right) Stimulation vs. time: Result from the reconstruction using optimal control (thick line) and reference stimulation $\overline{\sigma}$, see Eq. (17) applied in the experiments (dashed line). The relative muscle length is given by $l_{MTC}/l_{MTC,ref}=1$.

4 Discussion

4.1 Results for Muscle Length $\ell_{\text{MTC}} = \ell_{\text{MTC,ref}}$

We start with a discussion about several general findings for a single muscle length $\ell_{\text{MTC}} = \ell_{\text{MTC,ref}} = 6.15$ cm. In Figure 1 we compare the optimal control results to the experimental and reference data.

First of all we notice that the shape of the reconstructed stimulation σ^* is similar to the reference stimulation $\overline{\sigma}$. The same holds true for the recomputed force F_{MTC}^* (bold line) compared to the experimental data \overline{F}_{MTC} (thin line) and the model output $F_{MTC}(\overline{\sigma})$ (dashed line).

However, the reconstructed stimulation starts to rise before the onset of the reference stimulation. This can be partly explained by the forces, see Figure 1. The curve for the experimental data shows a much steeper increase than both computed curves, the bold one for the optimal control results and the dashed one for the model output. To compensate for the slower rate of increase, the optimal control curve has to start at earlier times $t < t_{start}$. This is only possible if the stimulation σ also switches to 1 at earlier times.

Secondly, one may observe that the experimental results for the force show a slow decrease right after the peak of the force at $t \simeq 0.5 \, \text{s}$, although the muscle is still fully stimulated, see Figure 2. A mathematical explanation cannot be given, but this might indicate fatigue. However, this slight decrease of the experimental force data is responsible for the rather strange and unexpected

local peak of the optimal control stimulation at time $t \simeq 1\,\text{s}$. Since the experimental forces decay already for $t > 0.5\,\text{s}$ and the optimal control tries to determine the stimulation such that the computed force fits the experimental data, the stimulation starts to decrease at around $t = 0.8\,\text{s}$.

Adjusting the decay rate of the computed force to the experimental data, in combination with the prior decay in the stimulation, seems to require the local peak of σ at t \simeq 1 s. Once the stimulation is switched off at times t > 1.1 s, all three force curves show almost identical decay rates. This indicates the model's good correspondence with its parameters and the real-world situation. The optimal control results are largely independent of the initial guess $\sigma_0(t)$; the presented results were obtained using $\sigma_0(t) \equiv 0.5$.

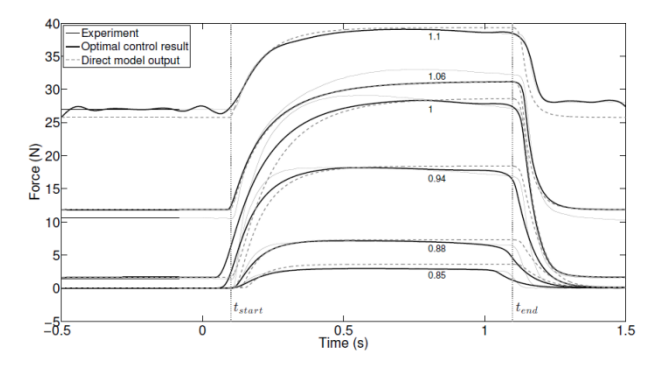


Figure 2 Isometric contraction forces vs. time: Experimental data from [29] (thin black line), optimal control results (bold black line) and direct model output using Eq. (14) (dashed line). The different graphs refer to different relative muscle lengths $\ell_{MTC}/\ell_{MTC,ref}$, marked with little numbers 0.85,..., 1.1..

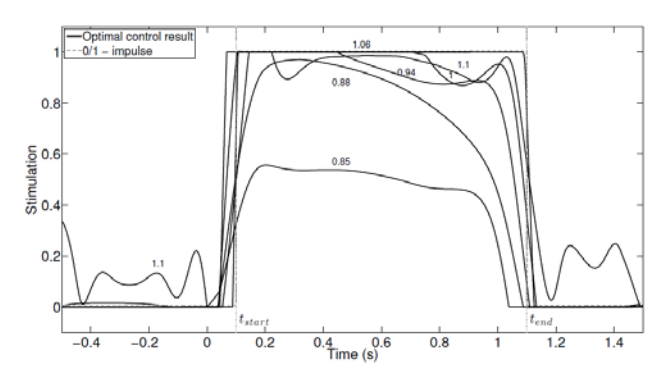


Figure 3 Stimulation vs. time for different muscle lengths: Result from the reconstruction using optimal control (thick line) and literature reference $\overline{\sigma}$, see [22] (dashed line). The muscle length is indicated by the $\ell_{MTC}/\ell_{MTC,ref}$ -ratio and printed besides the respective optimal control curves.

4.2 Results for Muscle between $0.85 \le \ell_{MTC}/\ell_{MTC,ref} \le 1.1$

Using Figures 2 and 3 we compare the optimal control results with the experimental and reference data for various muscle lengths given in [22].

The previously stated results for the shape of the calculated curves, the stimulation peak at t=1 sand the fatigue still hold true. However, the variation of the muscle length reveals some additional observations.

At short muscle length the stimulation σ in Figure 3 appears to be significantly lower than the expected full stimulation, e.g. $\sigma < 0.6$ at the shortest length $\ell_{\text{MTC}}/\ell_{\text{MTC,ref}} = 0.85$. An explanation cannot be given within the framework of the used models. However, this observation suggests replacing Zajac's activation dynamics Eq. (6) by Hatze's formula, see [26,30]. In this modified activation dynamics, the muscle activation q depends not only on the neural stimulation σ , but also on the current muscle length ℓ_{CE} .

For short muscles, e.g. $\ell_{\text{MTC}}/\ell_{\text{MTC,ref}} = 0.85$ and 0.88, the experimental data show a faster decay of the force compared to the simulated results. This may also indicate that the activation depends on the muscle length as explained above.

For long muscles, e.g. $\ell_{MTC}/\ell_{MTC,ref}=1.1$, Figure 3 shows, that the reconstructed stimulation is non–zero even for times $t < t_{start}$, which can be explained regarding the initial forces in Figure 2. For $t < t_{start}$ the experimentally observed forces are larger than the direct model output without neural stimulation. This indicates the need for further adjustment of the model parameters in the passive regime, i.e. for zero stimulation. The optimal control algorithm tries to diminish this force difference in order to reduce the objective function value. The only option is applying some non–zero stimulation to the model, which responds in generating the missing force for $t < t_{start}$.

The results for the muscle length $\ell_{MTC}/\ell_{MTC,ref}=1.06$ show a special behavior. Before the onset of the stimulation, i.e. for time $t < t_{start}$, the experimentally measured forces are less than the simulated forces, even with zero stimulation as seen in the direct model output (see dashed line in Figure 2). In contrast, the experimentally forces are larger than the simulated ones during the stimulation phase, i.e. for $t \in [t_{start}, t_{end}]$, even with maximal stimulation $\sigma = 1$. Hence the optimal control forces F_{MTC}^* agree with the model output $F_{MTC}(\overline{\sigma})$ for the experimentally applied 0/1-impulse $\overline{\sigma}$ in Eq. (17).

5 Comparison with Commercial Software

To further validate our findings, we present a comparison of the results obtained by our optimal control algorithm with a commercial software package called PROPT (see [31]). This software is based on MATLAB and available with a demo license. PROPT currently uses Gauss or Chebyshev–point collocation for solving optimal control problems. As initial input, PROPT uses the model functions Eq. (3)–(13) as well as the objective \Im and boundaries for state and control variables. The optimal control problem is discretized and the upcoming non-linear program (NLP) is solved. We are going to state some relevant facts using PROPT. For further information including some illustration problems see [32]. A similar commercial software package based on Gaussian pseudo-spectral collocation is called GPOPS2, see [14].

Since non–continuous functions cannot be handled by the above mentioned packages, we have to approximate the Heaviside function by a smooth function $\Theta_k(x) = \frac{1}{1+e^{-2kx}}$, with $k \gg 1$. In our computations k = 3000 turned out to be a good choice. Since the commercial packages solve the optimal control problem by a *first discretize then optimize* approach, attention has to be paid to the number of discretization or grid points used in the computations. For more than 200 grid points PROPT issued a warning that the upcoming NLP matrix was close to singularity and for less than 100 grid points the results may be incorrect. With a choice of 120 grid points the algorithm was able to run all calculations while the evaluation time was similar to our optimal control algorithm.

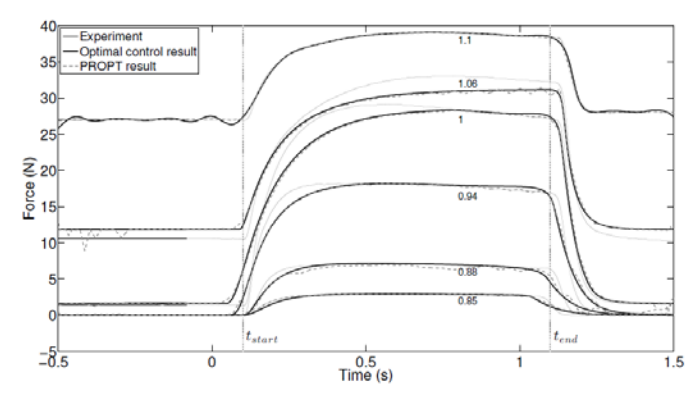


Figure 4 Isometric contraction forces vs. time: Experimental data (thin line), our Algorithm 1 (bold line) and software package PROPT (dashed line). The different graphs refer to different relative muscle lengths $\ell_{MTC}/\ell_{MTC,ref}$, compare Figure 2.

In Figure 4 we compare the computed muscle force obtained by our optimal control Algorithm 1 (bold line) and the PROPT–software (dashed line). As a reference we also included the experimental data (thin line). Figure 5 shows the stimulation σ computed by PROPT in comparison to the reference 0/1–impulse used in the experiments.

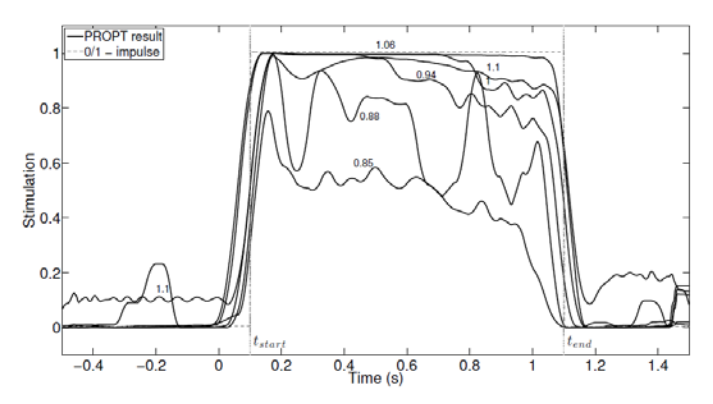


Figure 5 Stimulation vs. time for different muscle lengths: Result from the reconstruction using PROPT (thick line) and literature reference $\overline{\sigma}$, see [22] (dashed line). The PROPT result is smoothed by a moving average (over a time period dt = 0.08 s) to remove highly oscillatory behavior.

Both optimal control methods, our *first optimize then discretize* approach in Algorithm 1 and the *first discretize then optimize* method implemented in the PROPT software yield very similar results for the muscle forces, see Figure 4. The initial oscillations in the PROPT–force for the $\ell_{\text{MTC}}/\ell_{\text{MTC,ref}} = 1.06$ –curve can be explained by similar reasons as the optimal control results in the previous section.

Note that the stimulation σ computed by PROPT needed to be smoothed by a moving average filter. Due to the *first discretize then optimize* approach, the underlying NLP computes an individual optimal search direction for the stimulation σ at each discretization point. Hence the results can exhibit artificial oscillations and peaks. In contrast to that, our Algorithm 1, which is based on the *first optimize then discretize* approach, computes globally valid search directions; hence the results do not show discretization dependent artifacts or oscillations.

Table 1 lists the values of the objective function \Im , see Eq. (18), for our optimal control Algorithm 1, the commercial software PROPT and the direct model output using the 0/1-impulse stimulation. As expected, both optimized results yield lower objective function values compared to the direct output given in the

last column. Comparing the two optimization approaches to each other, the optimal control results are in most cases slightly better than the PROPT results; the total value of the objective function is about 3% lower for the optimal control methods.

Table 1 Objective function values at different muscle lengths: Optimal control Algorithm 1 (F_{MTC}^*), commercial software PROPT ($F_{MTC,P}$) and direct model output ($F_{MTC}(\overline{\sigma})$). Weighting parameter $\alpha = 0.1$. The fourth column shows the L^2 -difference between our results and the PROPT–results.

Length $\frac{\ell_{\text{MTC}}}{\ell_{\text{MTC,ref}}}$	Optimal Control $\mathcal{J}(F_{MTC}^*, \sigma^*)$	$\begin{array}{c} \textbf{PROPT} \\ \boldsymbol{\mathcal{J}}(\textbf{F}_{\textbf{MTC},\textbf{P}}, \boldsymbol{\sigma}_{\textbf{P}}^*) \end{array}$	Comparison $ \frac{1}{2} \ F_{MTC} - \overline{F}_{MTC}\ _{L^{2}} + \frac{\alpha}{2} \ \sigma^{*} - \sigma_{P}^{*}\ _{L^{2}} $	Direct Output $\mathcal{J}(F_{MTC}(\overline{\sigma}), \overline{\sigma})$
		2.0		10.1
0.85	3.3	2.9	1.9	13.4
0.88	7.6	8.7	6	15.0
0.91	9.7	8.9	4.8	24.0
0.94	15.3	15	6	28.1
0.97	16.5	17.2	5.4	35.3
1.00	22.9	24.2	4.2	33.8
1.03	24.7	26.3	4.4	32.7
1.06	24.8	25.9	6.1	26.4
1.08	8.9	9.4	3.6	21.0
1.10	4.9	3.3	3.2	21.8
Σ	138.6	141.9	45.6	251.5

6 Outlook and Future Research

We presented an optimal control algorithm to recalculate the stimulation of a muscle based on its isometric force output. Simulations performed with experimental data showed the applicability of our approach. High congruence between the experimentally applied stimulation and the mathematically recovered stimulation was found. A further comparison with commercial software validated our results. The computational results showed that the choice of the activation dynamics can be of importance. To further investigate the choice of activation dynamics, we derived a comparative sensitivity analysis of Hatze's and Zajac's activation dynamics by taking the effects of parameter changes into account, see [27].

Furthermore, a parameter estimation of the whole muscle model described in Chapter 2.1 would be of interest. In today's biomechanics parameter estimation is still done by educated trial and error, therefore we want to find an algorithmic optimization approach. The available models might be improved by including physiologically observed effects such as eccentric force-velocity relation, force depression, force enhancement and fatigue, see [21,33,34].

Eventually regarding modern biomechanical simulations we have to face huge multi-body systems with a multitude of muscles and boundary conditions performing a variety of movements such as walking, jumping or scoring a soccer goal, see [2,4,35,36]. Solving an optimal control problem for each muscle would be too expensive to perform within reasonable time. As an alternative optimal control strategy, the technique of *space-mapping* could be used. Developed for the use of microwave filter designs, see [37], the optimal control algorithm is based on the idea of two given models: an accurate but complex model and a simpler but inexact model. The optimization is done exclusively on the level of the simple model, whereas the crucial part is to find a mapping of the complex model to the simple model, the so-called *space-mapping*. This idea could be used to control a complex multi-body system with several hundreds of components.

Acknowledgment

The authors want to thank Dr. Michael Günther, University of Stuttgart for numerous discussions and providing us contact to experimenters. Special thanks also go directly to Prof. Dr. Veit Wank, University of Tübingen, for granting us access to his experimental results.

References

- [1] Tröltzsch, F., *Optimal Control of Partial Differential Equation*, **2**, Vieweg + Teubner, 2009 (Text in Germany).
- [2] Happee, R., Inverse Dynamic Optimization Including Muscular Dynamics, a New Simulation Method Applied to Goal Directed Movements, J. Biomechanics, 27(7), pp. 953-960, 1994.
- [3] Kistemaker, D.A., van Soest, A.J. & Bobbert, M.F., *Is Equilibrium Point Control Feasible for Fast Goal-Directed Single-Joint Movements?*, Journal of Neurophysiology, **95**(5),pp. 2898-2912, 2006.
- [4] Spägele, T., Kistner, A. & Gollhofer, A., A Multi-Phase Optimal Control Technique for the Simulation of a Human Vertical Jump, J. Biomechanics, **32**(1), pp. 87-91, 1999.
- [5] Höpler, R., Stelzer, M. & von Stryk, O., *Object-Oriented Dynamics Modeling for Legged Robot Trajectory Optimization and Control.* Proc. IEEE Conference on Mechatronics and Robotics, pp. 972-977, 2004.
- [6] Anderson, F.& Pandy, M., Static and Dynamic Optimization Solutions for Gait Are Practically Equivalent, J. Biomechanics, **34**(2),pp. 153-161, 2001.

- [7] Maas, R., Siebert, T. & Leyendecker, S., On the Relevance of Structure Preservation to Simulations of Muscle Actuated Movements, Biomech Model Mechanobiol., 11(3-4), pp. 543-556, 2012.
- [8] Buchanan, T. S., Estimation of Muscle Forces and Joint Moments Using a Forward-Inverse Dynamics Model, J. American College of Sports Medicine (ACSM), pp. 1911-1916, 2005.
- [9] Stelzer, M., & von Stryk, O., Efficient Forward Dynamics Simulation and Optimization of Human Body Dynamics, ZAMM, **86**(10), pp. 828-840, 2006.
- [10] Ghobadi, K., *On the Discretize then Optimize Approach*, Preprint for Industrial and Systems Engineering, 2009.
- [11] Heinkenschloss, M., *PDE Constrained Optimization*, Presentation at SIAM Conference, 2008.
- [12] Oberle, H.J., *Variational Calculus and Optimal Control*, Lecture, Department of Mathematics, University of Hamburg, 2008.
- [13] von Stryk, O., Numerical Solving of Optimal Control Problems: Discretizing, Parameter Optimization and Calculation of the Adjoint Variables., 8(441). VDI-Verlag, 1995 (Text in Germany).
- [14] RP Optimization Research LLC,http://www.gpops2.com/News/News, (20thJanuary 2015).
- [15] Tomlab Optimization Inc., http://www.tomopt.com/scripts/register, (20th January 2015).
- [16] Oberle, H.J. & Grimm, W., *BNDSCO-A Program for the Numerical Solution of Optimal Control Problems*, Institute for Flight Systems Dynamics, DLR, Oberpfaffenhofen, 1989.
- [17] Hinze, M., *Mathematics of PDE Constrained Optimization Discrete Concepts*, Presentation at Oberwolfach Seminar, 2010.
- [18] Pandy, M., Zajac, F., Levine, W. & Sim, E., *An Optimal Control Model for Maximum-Height Human Jumping*, J. Biomechanics, **23**(12),pp. 1185-1198, 1990.
- [19] Till, O., Characterization of Isovelocity Extension of Activated Muscle: A Hill-Type Model for Eccentric Contractions and a Method for Parameter Determination, Journal of Theoretical Biology, **225**(2), pp. 176-187, 2008.
- [20] Böl, M., A Finite Element Approach for the Modeling of Skeletal Muscle Fatigue, GAMM-Mitt., **32**(2), pp. 205-220, 2009.
- [21] Häufle, D., *Hill-Type Muscle Model with Serial Damping and Eccentric Force-Velocity Relation*, J. Biomechanics, **47**(6), pp. 1531-1536, 2014.
- [22] Günther, M., Schmitt, S. & Wank, V., *High-Frequency Oscillations as a Consequence of Neglected Serial Damping in Hill-Type Muscle Models*, Biological Cybernetics, **97**, pp. 63-79, 2007.

- [23] Siebert, T. & Rode, C. & Herzog, W., Nonlinearities Make a Difference: Comparison of Two Common Hill-Type Models with Real Muscle, Biol. Cybernetics, **98**(2),pp. 133-143, 2008.
- [24] van Soest, A. J., *Jumping from Structure to Control A Simulation Study of Explosive Moments*, Ph.D Thesis, Faculteit der Bewegingswetenschappen, Universiteitte Amsterdam, 1992.
- [25] Zajac, F. E., Muscle and Tendon: Properties, Models, Scaling, and Application to Biomechanics and Motor Control, Crit. Rev. Biomed. Eng, 17(4), pp. 359-411, 1989.
- [26] Hatze, H., *A Myocybernetic Control Model of Skeletal Muscle*, Biological Cybernetics, **25**(2), pp. 103-119, 1977.
- [27] Rockenfeller, R., Günther, M., Schmidt, S. & Götz, T., *Comparative Sensitivity Analysis of Muscle Activation Dynamics*, Accepted in Hindawi CMMM, 2015.
- [28] Hill, A. V., The Heat of Shortening and the Dynamic Constants of Muscle, Proceedings of The Royal Society London B, 126(843), pp. 136-195, 1938.
- [29] Wank, V., Muscle Growth and Fiber Type Composition in Hind Limb Muscles During Postnatal Development in Pigs, Cells Tissues Organs, **182**(243), pp. 171-81, 2006.
- [30] Günther, M., Computer Simulation for the Synthesis of Muscular Generated Human Walking of a Biomechanical Multi-Body-System, Ph.D Thesis, Department of Physics, Universität Tübingen, 1997. (Text in German).
- [31] Tomlab Optimization Inc., http://www.tomdyn.com/matlab_optimal_control_examples.html, (23th January 2015).
- [32] Rutquist, P., & Edvall, M., *PROPT Matlab Optimal Control Software*. TOMLAB Optimization Inc., 2010.
- [33] Kostarina, N., & Eriksson, A., *History Effect and Timing of Force Production Introduced in a Skeletal Muscle*, Biomech Modell Mechanobiol, **11**(7), pp. 947-957, 2012.
- [34] Till, O., Siebert, T., & Blickhan, R., Force Depression Decays During Shortening in the Medial Gastrocnemius of the Rat, J. Biomechanics, 47(5), pp. 1099-1103, 2014.
- [35] Menegaldo, L., A 'Cheap' Optimal Control Approach to Estimate Muscle Forces in Musculoskeletal Systems, J. Biomechanics, 39(10), pp.1787-1795, 2006.
- [36] Thelen, D., Using Computed Muscle Control to Generate Forward Dynamic Simulation of Human Walking from Experimental Data. J. Biomechanics, 39(3), pp. 1107-1115, 2006.
- [37] Koziel, S. & Bandler, J., "Accelerated Microwave Design Optimization With Tuning Space Mapping, IEEE Transactions on Microwave Theory and Techniques, 57(2), pp. 383-394, 2009.

Appendix A. List of Symbols

Symbol	Meaning	Value / Remark
a _{rel,0} /b _{rel,0}	Hill-parameters of contraction dynamics	0.1 resp. 1Hz (muscle-specific)
β	corresponding deactivation boost	0.8 (muscle-specific)
С	maximal Ca ²⁺ -concentration in Hatze (1977)	$1.37\cdot 10^{-4}\text{mol}\cdot l^{-1}$
\mathbf{D}_{SE}	damping parameter	0.3 (muscle-specific)
ΔW_{asc}	width of ascending limb of Fisom-curve	0.57 (muscle-specific)
ΔW_{des}	width of descending limb of Fisom-curve	0.14 (muscle-specific)
$\Delta F_{SEE,0}$	reference force of SEE	60N (muscle-specific)
$\Delta U_{SEE,nll}$	relative width of non-linear branch in SEE	0.1825 (muscle-specific)
$\Delta U_{SEE,l}$	relative width of linear branch in SEE	0.073(muscle-specific)
F_e	limit factor for eccentric Force	1.8 (muscle-specific)
F _{isom}	isometric muscle force	length-depending
$\mathbf{F}_{\mathbf{max}}$	maximum isometric force of the CE	30N (muscle-specific)
$oldsymbol{\mathcal{F}}_{ ext{PEE}}$	normalization factor of F _{PEE} w.r.t. F _{max}	1 (muscle-specific)
γ	representation of free Ca ²⁺ -concentration	time-depending
$\ell_{ ext{CE}}$	contractile element length	time-depending
$\dot{m{\ell}}_{ extsf{CE}}$	contraction velocity	first time derivative of $\ell_{\rm CE}$
$\ell_{ ext{CEopt}}$	optimal CE length	0.015m (muscle-specific)
\mathcal{L}_{PEE}	root of F_{PEE} at $\mathcal{L}_{PEE} \ell_{CEopt}$	0.9 (muscle-specific)
$\ell_{\rm o}$	pole in Hatze's length dependency function	2.9
$\ell_{ ext{SEE},0}$	slack length of SEE	0.045m (muscle-specific)
m	activation frequency constant in Hatze	10 Hz (muscle-specific)
ν	exponent in Hatze's formulation	3 (muscle-specific)
v_{asc}	exponent of ascending limb of F _{isom} -curve	4 (muscle-specific)
$v_{ m des}$	exponent of descending limb of F _{isom} -curve	3 (muscle-specific)
ν_{PEE}	exponent of F _{PEE} -curve	2.5 (muscle-specific)
q	muscle activity (bound Ca ²⁺ -concentration)	time-depending
$\mathbf{q_0}$	basic activity according to Hatze (1977)	0.005
$\mathbf{q}_{\mathbf{H}}$	activation dynamics from Hatze	time-depending
R_{SE}	damping parameter	0.01 (muscle-specific)
ρ	length dependency of Hatze's activation	length-depending
$ ho_0$	factor in van Soest (1992) and Hatze (1977)	$5.27 \cdot 10^4 \text{ mol } l^{-1} \text{ (muscle-specific)}$
S_e	ratio of derivatives of F_{CE} at $\dot{\ell}_{CE} = 0$	2 (muscle-specific)
σ	neural muscle stimulation	time-depending
τ	activation time constant	here: $\frac{1}{40}$ s